Biochimica et Biophysica Acta 1859 (2017) 1941–1950

Contents lists available at ScienceDirect

Biochimica et Biophysica Acta

journal homepage: www.elsevier.com/locate/bbamem

Probing the disparate effects of arginine and lysine residues on antimicrobial peptide/bilayer association

A. Rice, J. Wereszczynski*

Department of Physics and The Center for Molecular Study of Condensed Soft Matter, Illinois Institute of Technology, Chicago, Illinois 60616, USA

ARTICLE INFO

Article history:
Received 2 February 2017
Received in revised form 8 May 2017
Accepted 1 June 2017
Available online 3 June 2017

Keywords:
Molecular dynamics simulations
Antimicrobial peptides
Peptide-bilayer interactions
KR-12

ABSTRACT

Antimicrobial peptides (AMPs) are key components of the innate immune response and represent promising templates for the development of broad-spectrum alternatives to conventional antibiotics. Most AMPs are short, cationic peptides that interact more strongly with negatively charged prokaryotic membranes than net neutral eukaryotic ones. Both AMPs and synthetic analogues with arginine-like side chains are more active against bacteria than those with lysine-like amine groups, though the atomistic mechanism for this increase in potency remains unclear. To examine this, we conducted comparative molecular dynamics simulations of a model negatively-charged membrane system interacting with two mutants of the AMP KR-12: one with lysine residues mutated to arginines (R-KR12) and one with arginine residues mutated to lysine (K-KR12). Simulations show that both partition analogously to the bilayer and display similar preferences for hydrogen bonding with the anionic POPGs. However, R-KR12 binds stronger to the bilayer than K-KR12 and forms significantly more hydrogen bonds, leading to considerably longer interaction times. Additional simulations with methylated R-KR12 and charge-modified K-KR12 mutants show that the extensive interaction seen in the R-KR12 system is partly due to arginine's strong atomic charge distribution, rather than being purely an effect of the greater number of hydrogen bond donors. Finally, free energy simulations reveal that both peptides are disordered in solution but form an amphipathic α-helix when inserted into the bilayer headgroup region. Overall, these results highlight the role of charge and hydrogen bond strength in peptide bilayer insertion, and offer potential insights for designing more potent analogues in the future.

1. Introduction

The emergence of drug resistant bacteria poses a major threat to modern medicine and has prompted the search for alternatives to conventional antibiotics. Antimicrobial peptides (AMPs), small peptides produced by many different organisms as part of the innate immune system, are of great research interest both for their ability to stimulate the innate immune system, as well as their broad spectrum of antimicrobial activity against Gram-positive and Gram-negative bacteria, viruses, and parasites [1–3]. AMPs typically adopt amphipathic structures when interacting with cell membranes, and often contain a high proportion of cationic residues [1,4,5], which interact strongly with the anionic lipids characteristic of bacterial membranes. There are many different mechanisms to explain the ability of AMPs to selectively disrupt cell membranes, including the carpet/detergent model, pore formation, anionic lipid clustering, and direct membrane translocation [3–6].

Both AMPs and their relatives, cell penetrating peptides (CPPs) tend to contain a large fraction of arginine and lysine residues, with arginine more prevalent than lysine [7]. Though the two residues have the same net charge, switching the guanidinium groups of arginine for the amine groups of lysine has been shown to decrease the antimicrobial activity, membrane disruptive ability, and cytotoxicity for many AMPs [7–10], including tritrpticin [6,11], human neutrophil peptide 1 [12], and KR-12 [13]. Likewise, synthetic peptidomimetics containing amine side chains were shown to be less active against eight bacterial strains than those containing guanidinium groups and, unlike their guanidinium-containing counterparts, do not disrupt DPPG monolayers [14]. Studies comparing arginine and lysine oligomers have shown that polyarginine enters cells far more efficiently than polylysine [15], and binds more strongly to both POPC and mixed POPC/POPG bilayers [16]. This disparity in activity is often attributed to the greater hydrogen bonding capacity of arginine than lysine, and the importance of hydrogen bonding in bilayer association, translocation, and disruption. There are, however, other differences between the two residues aside from the number of hydrogen bond donors: lysine is slightly more hydrophobic than arginine, is a weaker base with a lower pK_a, contains a more localized

* Corresponding author.
E-mail address: jwereszc@iit.edu (J. Wereszczynski).

http://dx.doi.org/10.1016/j.bbamem.2017.06.002
0005-2736/

cationic charge than arginine, and has weaker partial charges on its nitrogen and hydrogen atoms.

Human cathelicidin LL-37 is a 37 residue α-helical AMP that is active against Gram-positive and Gram-negative bacteria [17,18], and believed to function through the carpet mechanism [19–22]. In addition to its bacteriocidal properties, LL-37 modulates the innate immune response through its chemoattractant properties and by stimulating the release of interleukin 8 (IL-8) and other chemokines to further attract neutrophils and monocytes to the infection site [2,18,23]. LL-37 is also able to bind to and neutralize lipopolysaccharide (LPS) [18,24,25], which helps protect the body against one source of septic shock. Despite these unique properties that make LL-37 an appealing template for future drug design, LL-37 is significantly hemolytic and cytotoxic to human cells [18,26-28]. KR-12 is a truncated portion of LL-37 corresponding to residues 18-29 (sequence KRIVQRIKDFLR), and is the smallest section of the peptide that is as active as LL-37 against Gram-negative [13,28,29] and certain Gram-positive bacteria [28]. More importantly, KR-12 is much less cytotoxic and hemolytic than LL-37 [13,28,29], though it does not retain the LPS-neutralizing properties of its parent peptide [28].

Here, we present a series of molecular dynamics (MD) simulations designed to elucidate the source of the different effects of arginine and lysine on AMP/bilayer interactions, with an emphasis on the first step of membrane disruption: the initial attraction to and insertion of peptides to the bilayer. The interactions of four KR-12 variants with model neutral and negatively charged bilayers were simulated. These included peptides in which the five cationic KR-12 residues were mutated to arginines and lysines (R-KR12 and K-KR12 respectively), as well as variants with monomethylarginines (mR-KR12), asymmetric dimethylarginines (dmR-KR12), and charge-mutated lysines (mutK-KR12). Arginine methylations were performed to examine the effects of hydrogen bonding, since methylation does not significantly alter the pK_a or electrostatic potential of the remaining hydrogen atoms but does alter the number of available hydrogen bond donors [30].

Simulations show that both peptides partition analogously to the bilayer and display similar preferences for forming hydrogen bonds with the anionic POPGs. However, R-KR12 has a significantly higher propensity for hydrogen bonding with the bilayer than K-KR12, as well as stronger peptide-bilayer binding, resulting in considerably longer interaction times. Additional simulations with the mutant R-KR12 and K-KR12 peptides show that the differing number of hydrogen bond donors alone does not account for these distinct interactions, and that the strength of atomic partial charges strongly influences peptide-bilayer affinity. Finally, free energy simulations reveal that both peptides are similarly affected by the presence of the bilayer and adopt a highly helical amphipathic structure when inserted into the bilayer headgroup region, indicating that observed helicity differences in these simulations are an effect of bilayer binding rather than residue side chain identity.

2. Materials/methods

2.1. System preparation

Initial coordinates of a POPC bilayer containing 48 lipids in each leaflet and a 3:1 POPC:POPG bilayer containing 36 POPC and 12 POPG per leaflet were generated using the CHARMM-GUI membrane builder [31,32] and the CHARMM 36 (C36) lipid force field [33,34]. The solvate and autoionize plugins of VMD [35] were used to add ~15 Å TIP3P water [36] with 0.15 M NaCl in the ± z dimensions. Next, the parameter and coordinate files were converted to AMBER-compatible format using chamber [37] in ParmEd. Both bilayers were minimized for 20,000 steps, heated to 310 K over 60 ps, then simulated for 5 ns in the NPT ensemble with 10 kcal/(mol·Å ^{2}) restraints to allow the water to reach an appropriate density. Finally, both bilayers were simulated for 200 ns in the NPT ensemble, using the simulation parameters described below. Final frames from these simulations, referred to as the equilibrated bilayers, were used to construct the peptide-bilayer systems detailed below. The POPC/POPG bilayer simulation was later extended to 1.0 μs to ensure equal sampling for bilayer thickness map calculations.

Five mutants of the KR-12 peptide (PDB: 2K6O) [29] were constructed by changing all five of the cationic residues (Fig. 1a) to either lysine, arginine, monomethylarginine, symmetric dimethylarginine, or charge-mutated lysine (referred to as K-KR12, R-KR12, mR-KR12, dmR-KR12, and mutK-KR12 respectively). These peptides were used to construct seven systems (Table 1) with the equilibrated POPC and POPC/POPG bilayers described above. The peptide was initially placed on one side of the bilayer, with the center-of-mass (COM) about 25 Å from the bilayer surface (Fig. 1b), in three different tilt orientations relative the the bilayer surface: 0° and ± 30°. All systems were prepared using the C36 force fields for proteins [38,39] and lipids [33,34], with modified Lennard-Jones parameters for sodium ion interactions with certain lipid oxygens [40], then converted to AMBER-compatible formats as described above. Side chains of the two modified arginine residues (Fig. 1c) were parameterized following the general CHARMM procedure [41] using the Force Field Toolkit (ffTK) [42] plugin in VMD, using a simulated annealing protocol [43] to fit to target quantum mechanical data generated with Gaussian 09 [44]. Further parameterization details and optimized atomic partial charges for methylarginine and symmetric dimethylarginine are given in Section S1.1 and Table S1 in the Supporting Material. Atomic charges of the mutated lysine residue where changed by hand (Table S2) to replicate those found in arginine, and all other parameters were unchanged.

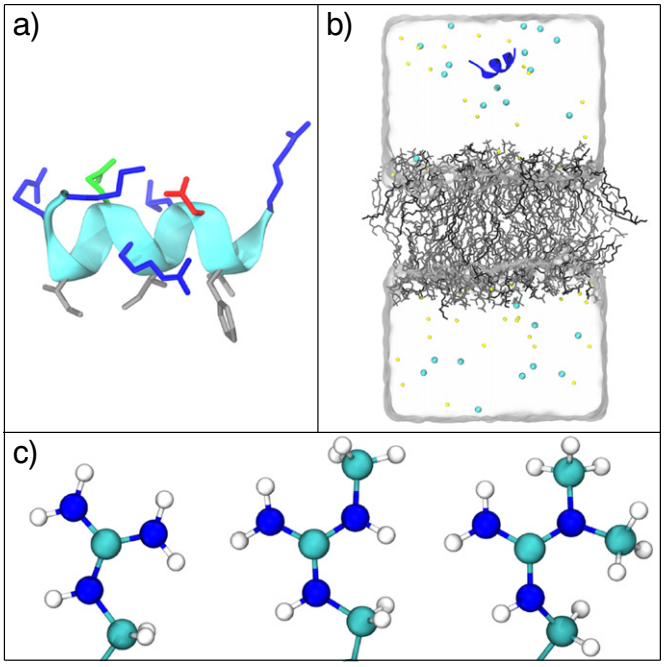

Fig. 1. a) Structure of the model AMP KR-12; side chains are colored blue for cationic residues, red for anionic residues, gray for hydrophobic residues, and green for polar uncharged residues. b) the R-KR12/POPC/POPG simulation box. POPC and POPG are shown in gray and black, respectively, with hydrogen atoms removed for clarity. R-KR12 is shown in the cartoon representation, with sodium and chlorine ions displayed as colored spheres and water molecules shown as a transparent box. c) Terminal portion of the arginine (left), methylarginine (center), and asymmetric dimethylarginine (right) side chains.

Table 1
List of all peptide-bilayer simulations performed in this study. *One R-KR12/POPC/POPG simulation was extended to 2.0 μs.

Peptide	Type	Bilayer	Number of simulations	Length per simulation (ns)
K-KR12	cMD	POPC	3	500
		POPC/POPG	3	500
	US	—	180	25
		POPC/POPG	180	50
R-KR12	cMD	POPC	3	500
		POPC/POPG	3	500*
	US	—	180	25
		POPC/POPG	180	50
mutK-KR12	cMD	POPC/POPG	3	500
dmR-KR12	cMD	POPC/POPG	3	500
mR-KR12	cMD	POPC/POPG	3	500

2.2. Molecular dynamics simulations

Initial equilibration was performed in both the NVT and NPT ensembles, with a 2 fs time step and restraints on the lipid headgroup and peptide backbone atoms. Before the equilibration phase, systems were energy minimized using both the steepest descent and conjugate gradient algorithms, with 10 kcal/(mol·Å^2) restraints on the lipid headgroup and peptide backbone atoms. In the equilibration phase, systems were first heated in the NVT ensemble to 310 K over 50 ps, followed by 1 ns in the NPT ensemble to allow the density of the solvent to equilibrate. No restraints were applied during the NPT production phase, which was carried out for 500 ns in all systems (Table 1), except for one that was extended to 2.0 μs. Frames were saved every 10 ps during the production phase.

System temperatures were controlled at 310 K using Langevin dynamics, with a collision frequency of 1.0 ps^{-1}. The pressure was maintained at 1.0 bar by means of semi-isotropic coordinate scaling, with z decoupled from the xy dimensions, utilizing the Berendsen barostat [45] and a relaxation time of 1.0 ps. All hydrogen bonds were constrained using SHAKE [46]. AMBER 14, the version available at the start of this study, does not support a switching method for non-bonded interactions, so a hard cutoff of 10.0 Å was used, which has been shown to suitably reproduce C36 lipid properties [47]. Long-range electrostatics were treated with the particle mesh Ewald (PME) method [48] with a grid spacing of 1.0 Å. All conventional MD (cMD) simulations were performed with the GPU-accelerated version of *pmemd* in AMBER 14 [49].

2.3. Umbrella sampling calculations

Distinct helicity differences between K-KR12 and R-KR12 were observed in the cMD simulations (Section 3.1). To quantify whether these differences were due to preferential membrane binding or the presence of arginine/lysine, umbrella sampling (US) [50] simulations were performed to calculate two-dimensional potentials of mean force (PMFs) for K-KR12 and R-KR12, both free in solution and inserted in the headgroup region of the POPC/POPG bilayer. All US simulations were done in NAMD 2.11 [51], in order to utilize the alpha and distanceZ collective variables [52]. Since end-to-end distance alone may not be sufficient to characterize peptide folding [53], two reaction coordinates were used to define the conformational landscape of the peptides: alpha, a value between 0 and 1 that describes the α-helical content of a protein segment, and the end-to-end distance of the peptide, measured from the N-terminal nitrogen to the C-terminal carbon. Initially, eighty-one independent simulations (windows) were used, with the alpha collective variable ranging from 0.1 to 0.9 in increments of 0.1, and the peptide end-to-end distance ranging from 6.0 Å to 38.0 Å in increments of 4.0 Å. These values were maintained by harmonic restraints of 1000 kcal/(mol ·U^2) for alpha and 0.4 kcal/(mol ·Å^2) for end-to-end distance, and windows were coupled to one another with a replica exchange US (REUS) protocol [54], with exchange attempted every 1000 steps. To improve overlap, following these simulations, the centers of each window were shifted by +0.05 in alpha and −2.0 Å in end-to-end distance to create eighty-one new windows, with alpha ranging from 0.15 to 0.95 in increments of 0.1, and the end-to-end distance ranging from 4.0 Å to 36.0 Å in increments of 4.0Å; the restraint force constants and exchange protocol were unchanged.

Each of the eighty-one initial windows was initiated from the same structure. Starting peptide coordinates for the simulations of K-KR12 and R-KR12 in solution were taken from a frame of the cMD peptide/bilayer simulations which had an alpha value of 0.64 and a distance of 17 Å for K-KR12, and 0.54 and 12 Å for R-KR12. Starting structures for the simulations of R-KR12 and K-KR12 inserted in the POPC/POPG bilayer were taken from a frame of the cMD simulation with R-KR12 inserted (COM = - 2.6 Å) in the headgroup region of the POPC/POPG bilayer, an alpha value of 0.76, and an end-to-end distance of 19Å; since K-KR12 did not insert as deeply as R-KR12 in conventional simulations, this same frame was used to start the K-KR12 windows as well following mutation of the arginines into lysines. In all four systems, poor sampling was observed in the 4–5 Å end-to-end distance range, so eighteen additional windows were added from the same initial structure, with the end-to-end distance centered at 4.5 Å and alpha ranging from 0.10 to 0.95 in increments of 0.05. Harmonic restraints on the end-to-end distance were increased to 2.5 kcal/(mol ·Å^2) to ensure the 4–5 Å region was well sampled. Since these windows were added following initial calculations, replica exchange was not performed.

In total, one hundred eighty windows were simulated per system (eighty-one initial REUS windows, eighty-one reinitialized REUS windows, and eighteen additional US windows). All US simulations were performed in the NPT ensemble, with the temperature controlled at 310 K using Langevin dynamics and the pressure controlled anisotropically at 1.0 bar using the Langevin piston Nosè-Hoover method [55]. A 10–12 Å force-based switching function was used for Lennard-Jones interactions, consistent with the switching range used to develop the C36 force field. Hydrogen bond constraints, long-range electrostatics, and simulation timesteps were treated as described above. Exchanges between adjacent windows were attempted every 1000 steps. In the case of the peptides free in solution, each window was simulated for 25 ns with the first 5 ns discarded as equilibration, resulting in a total of 3.6 μs of sampling per PMF. Due to the slower diffusive nature of lipids than water, each window in the case of the peptide inserted in bilayer was simulated for 50 ns, with the first 15 ns discarded, to allow the lipids to equilibrate fully around the peptide, resulting in a total of 6.3 μs sampling per PMF. Free energy profiles for each system were obtained using the weighted histogram analysis method [56,57], and the missing Jacobian contribution from the end-to-end distance was applied to obtain the true PMFs [58].

In simulations of K-KR12 inserted in the bilayer, the peptide had a tendency to drift out of the membrane if unrestrained; therefore, the windows with K-KR12 in the bilayer required an additional procedure to ensure the peptide stayed inserted in the headgroup region. The projection onto the z-axis of the distance between the peptide's COM and the bilayer COM was restrained with a half-harmonic potential, centered at 23.0 Å (corresponding roughly to a distance of 2 Å from the bilayer surface) with a force constant of 1.0 kcal/(mol ·Å^2). Since R-KR12 never left the bilayer in any of the REUS windows, no restraints were needed for this system. Analysis of the peptide-bilayer distance for both the restrained K-KR12 and unrestrained R-KR12 systems verified that both peptides indeed stayed inserted and sampled similar insertion depths (Figure S2).

2.4. Simulation analysis

Throughout this work, we defined a bilayer leaflet's position as the center of the phosphorus atoms in that leaflet. The peptide was defined as 'associated' with the bilayer if any of the peptide heavy atoms were within 5 Å of this leaflet position, and 'inserted' if the peptide's COM was below this leaflet position. The percent association was calculated as the number of trajectory frames where the peptide was associated with the bilayer, divided by the total number of frames. Hydrogen bonds between the peptide and lipids were calculated using the hbonds plugin of VMD, with a distance cutoff of 3.5 Å and an angle cutoff of 30°. All cMD trajectories were post-processed using the colvar module [52] of NAMD 2.11 to calculate the α-helical content of the peptide (using the collective variable alpha, described above) for each frame. Lipid bilayer thickness maps were calculated with the VMD plugin MEMBPLUGIN [59], using frames every 100 ps and a resolution of 1.0 Å. Lipid clustering and XY radial distribution functions (RDFs) were calculated using LOOS [60].

Finally, peptide-bilayer binding energies were estimated via the Molecular Mechanics/Generalized Born Surface Area (MM/GBSA) method, utilizing the MMPBSA.py script in AmberTools 14 [61], mbondi2 for the atomic radii, and the modified GB model developed by Onufriev et al. (igb=5) [62] to implicitly model solvent effects. Only portions of the trajectory where the peptide was associated with the bilayer were used for these calculations.

3. Results

3.1. Long-term bilayer interactions

Each system had distinct association properties with the bilayers studied here (see Table 2). Neither K-KR12 nor R-KR12 were found to form stable, long-term interactions with the pure POPC bilayer, with peptide-bilayer associations only present for 5% and 30% of the trajectories respectively. The time evolution of the peptide's center of mass (COM) distance to the bilayer surface (Fig. 2) shows that both peptides spent the majority of the simulation far from the bilayer surface, with typical bilayer associations representing chance encounters and lasting on the order of 1–10 ns for K-KR12 and 10–50 ns for R-KR12. While associated with the bilayer, K-KR12 primarily interacted with the POPC bilayer through the side chains of K1 and K2 (Table S3), resulting in a relatively large association distance of 12.4 ± 0.8 Å, which is defined as the peptide's average COM distance to the bilayer when associated (corresponding to the first plateau in Figure S3). On the other hand, R-KR12 interacted with the bilayer through all five arginine residues, leading to a COM distribution that is shifted closer to the bilayer (Figure S3), a closer association distance of 10.7 ± 0.5 Å, and significantly more peptide-bilayer hydrogen bonds (3.42 ± 0.61). Finally, despite being initialized in a highly helical state, both peptides unfolded quickly and maintained a semi-helical conformation during the course of the simulations, with average alpha values of 0.47 ± 0.16 for K-KR12 and 0.56 ± 0.15 for R-KR12 (Figure S4).

In contrast to the pure POPC bilayer, both K-KR12 and R-KR12 formed stable, long-term interactions with the mixed POPC/POPG bilayer. Both peptides spent the majority of the simulation time at the bilayer (62% association for K-KR12 and 88% for R-KR12) and had longer association times (Fig. 2). In the case of K-KR12, these associations persisted for tens to hundreds of ns, while in simulations with R-KR12 we did not observe a peptide dissociating from the bilayer once it had associated, even on the μs timescale (Figure S5). In addition, peptide insertion was very rare in the K-KR12 system, while R-KR12 inserted much more readily into the bilayer with insertion present in 9.3% of the peptide associated time. Additionally, in the simulation that was extended out to 2.0 μs, stable insertion was observed on the hundreds of ns timescale. Pore formation was not observed in these simulations, though the time scale needed to observe pore formation with the CHARMM36 lipid force field is likely orders of magnitude longer than the simulations performed here [63]. As in the simulations with the pure POPC bilayer, K-KR12 interacted with the POPC/POPG bilayer predominantly through residues K1 and K2 (Table S3), leading to similar average association distance and COM distributions (Fig. 3). R-KR12, however, was held much closer to the POPC/POPG bilayer than the pure POPC bilayer, with an average association distance of only 5.7 ± 1.3 Å. The R-KR12/POPG containing system had the largest number of peptide-bilayer hydrogen bonds, with an average of 5.97 ± 0.54 hydrogen bonds formed. Finally, K-KR12 stayed predominantly unfolded in these simulations, while R-KR12 maintained a helical structure (Figure S4). The source of this asymmetry was explored using the free energy calculations discussed below.

The increased binding strength of arginine over lysine containing peptides is likely due to one of two properties: the ability of arginines to form bidentate hydrogen bonds or the larger partial charges in arginines creating stronger peptide-bilayer hydrogen bonds. To decouple these effects, we performed simulations of peptides containing methylated arginines which have a decreased number of hydrogen bond donors but similar charge distributions to unmodified arginines, as well as simulations with peptides where the lysine side chains were mutated to have arginine-like charges. Many of the long-term bilayer interactions of mutK-KR12, dmR-KR12, and mR-KR12 with the POPG containing bilayer were similar to those of R-KR12, and stable interactions were observed in all nine simulations. mutK-KR12, dmR-KR12, and mR-KR12 had similar percent bilayer associations of 75%, 78%, and 82% respectively, and in a number of these simulations, the peptide remained associated with the bilayer after forming its first stable contact with the surface (Fig. 2), a behavior observed in R-KR12 but not K-KR12 systems. Additionally, the association and COM distribution distances of dmR-KR12 and mR-KR12 correspond more to those of R-KR12 than K-KR12, and both peptides interacted with the bilayer through all five cationic residues (Table S3). Interestingly, mutK-KR12 behaved more like K-KR12 in these measures. As with R-KR12, mR-KR12 inserted into the

Table 2
Interaction of KR12 with POPC and POPC/POPG. The percent association, average number of hydrogen bonds between the peptide and lipids, average lifetime of these hydrogen bonds, percentage of bidentate arginine hydrogen bonds, average association distance, percent insertion, average peptide helicity, and peptide-bilayer binding energy (MM/GBSA) are listed. Percent association and peptide helicity are calculated over the full trajectories, while association distance, percent insertion, number of hydrogen bonds, bidentate percentage, and binding energy are calculated only over the frames where the peptide is associated with the bilayer. All errors are reported as standard errors of the mean.

Peptide	Bilayer	Percent association	Hydrogen bonds	H-Bond lifetime (ps)	Bidentate percentage	Association distance (Å)	Percent insertion	Helicity (α)	Binding energy (kcal/mol)
K-KR12	POPC	5%	0.75 ± 0.22	92 ± 18	–	12.4 ± 0.8	0.0%	0.47 ± 0.16	1.2 ± 1.5
R-KR12	POPC	30%	3.42 ± 0.61	196 ± 10	36.7%	10.7 ± 0.5	0.0%	0.56 ± 0.15	−21.2 ± 4.1
K-KR12	POPC/POPG	62%	2.34 ± 0.20	135 ± 7	–	12.0 ± 0.5	0.2%	0.34 ± 0.15	−14.6 ± 1.9
mutK-KR12	POPC/POPG	75%	3.50 ± 0.22	251 ± 8	–	11.1 ± 0.4	0.0%	0.28 ± 0.15	−24.5 ± 1.9
dmR-KR12	POPC/POPG	78%	3.31 ± 0.22	261 ± 34	0.0%	7.5 ± 1.5	0.6%	0.53 ± 0.08	−26.7 ± 2.0
mR-KR12	POPC/POPG	82%	3.66 ± 0.29	231 ± 4	13.9%	7.1 ± 1.0	5.5%	0.56 ± 0.10	−28.2 ± 3.6
R-KR12	POPC/POPG	88%	5.97 ± 0.54	232 ± 14	35.6%	5.7 ± 1.3	9.3%	0.75 ± 0.06	−49.3 ± 4.4

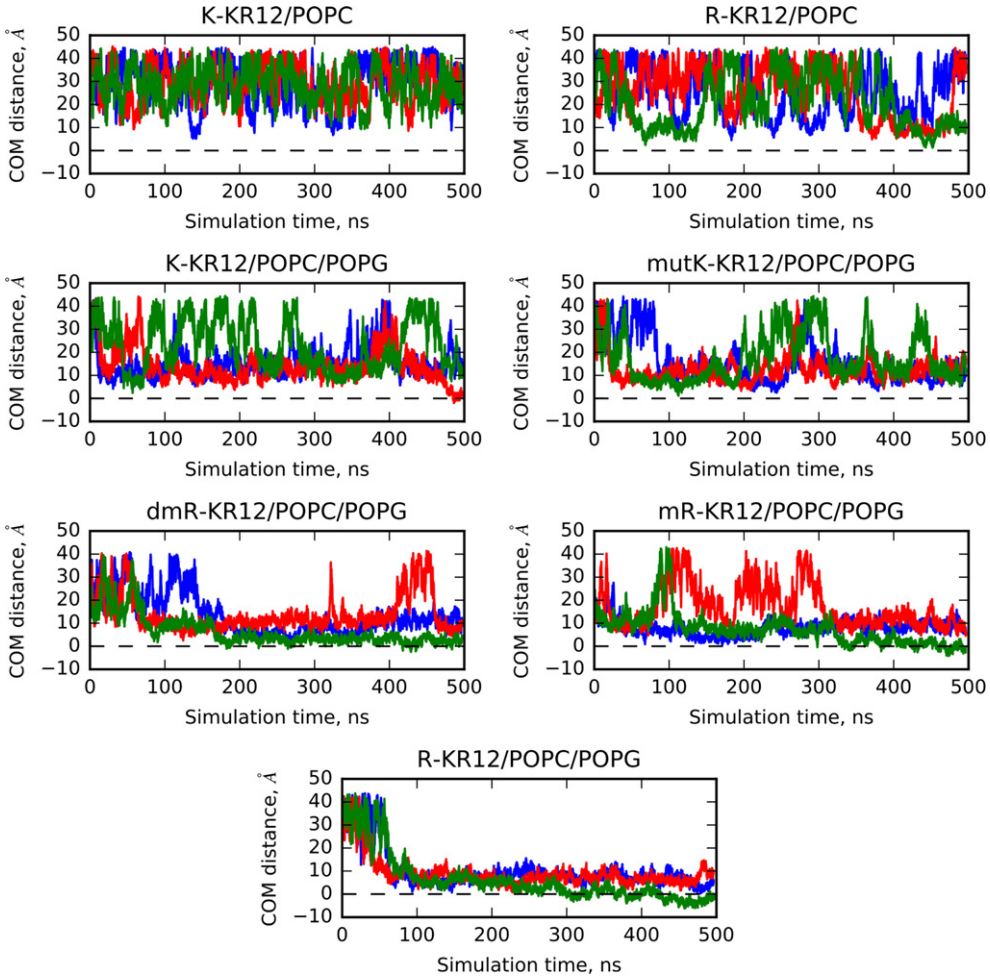

Fig. 2. Time evolution of the COM distance to the POPC and POPC/POPG bilayer for all five peptides. Different colors represent different initial peptide orientations for each simulation. Both K-KR12 and R-KR12 rarely interacted with the pure POPC bilayer, while interactions with the POPC/POPG bilayer were much more frequent and persistent.

bilayer fairly readily, with insertion observed 5.5% of the bilayer associated time, while dmR-KR12 only inserted 0.6% of this time. We note that methylating arginine increases its hydrophobicity [6,30] and has previously been shown to affect a peptide's ability to partition into the bilayer [12]. No insertion was observed in the mutK-KR12 simulations. Despite the many similarities between the methylated peptides and R-KR12, both mR-KR12 and dmR-KR12 maintained semi-helical conformations during the course of the simulations (Figure S4), instead of the highly helical conformation observed in the R-KR12 simulations. Like K-KR12, mutK-KR12 was primarily unfolded in these simulations.

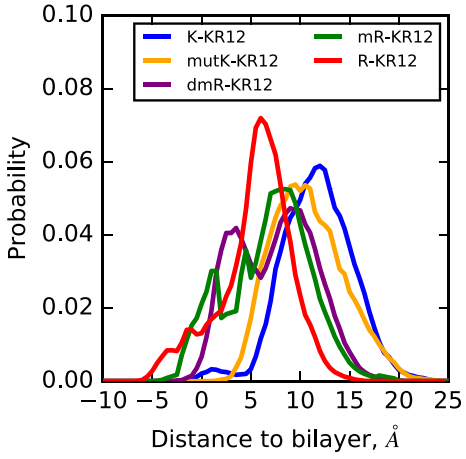

Fig. 3. Distribution of COM distances to the POPC/POPG bilayer, using only the portion of the simulation where the peptide is associated with the bilayer. K-KR12 rarely inserted into the bilayer and displayed a more extended association distance than the other four peptides.

3.2. Role of peptide-bilayer hydrogen bonding

All five peptides preferentially formed hydrogen bonds with the anionic POPG lipids over the neutral POPC ones (Fig. 4). Since POPG accounted for 25% of the mixed bilayer, if there were no preferential binding we would expect only ~25% of the hydrogen bonds to be formed by POPG. However, POPG hydrogen bonds constituted a significantly larger percentage of peptide-bilayer hydrogen bonds in each system. Additionally, both K-KR12 and R-KR12 formed significantly fewer hydrogen bonds with the pure POPC bilayer than with the POPC/POPG bilayer, which can be attributed to favorable electrostatic interactions of the positively-charged peptides with the anionic POPG.

R-KR12 formed more bilayer hydrogen bonds than K-KR12 for both systems, which can be ascribed in part to the greater number of hydrogen bond donors present in arginine than in lysine. Hydrogen bonding with one of arginine's terminal side chain nitrogen atoms was observed to promote the formation of additional (bidentate)

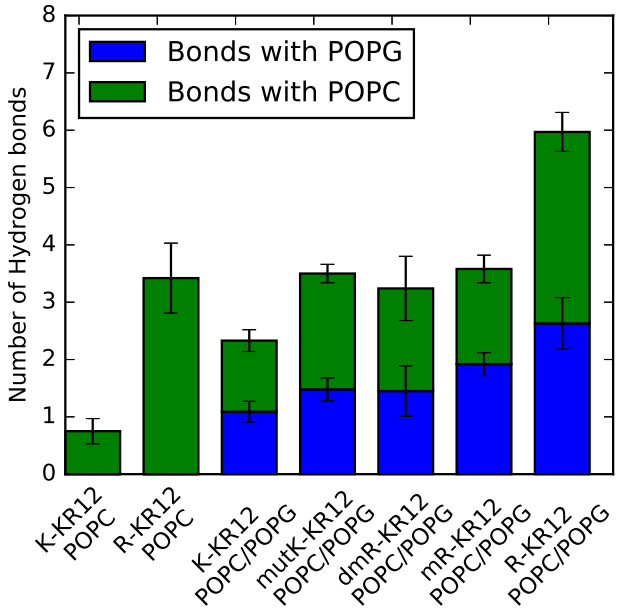

Fig. 4. Average number of hydrogen bonds formed while associated with the respective bilayers, shown as bonds with POPC or POPG. All five peptides showed a preference for binding with POPG, which constitutes only 25% of the bilayer, over POPC.

hydrogen bonds: R-KR12 formed bidentate hydrogen bonds 36.7% of the time in the case of the pure POPC bilayer and 35.6% of the time in the case of the POPC/POPG bilayer (Table 2). Introducing a single methylation (mR-KR12) led to a decrease in bidentate hydrogen bond formation (13.9%) and, predictably, the asymmetric dimethylation (dmR-KR12) completely eliminated bidentate hydrogen bonds. Interestingly, dmR-KR12 and mR-KR12 formed a comparable total number of hydrogen bonds with the bilayer, 3.31 ± 0.22 and 3.66 ± 0.29 respectively, despite this large difference in the ability to form bidentate bonds. mutK-KR12 also formed an intermediate number of hydrogen bonds with the bilayer, 3.5 ± 0.22. While asymmetric dimethylarginine and charge-mutant lysine have the same number of hydrogen bond donors as lysine, both formed statistically significantly more hydrogen bonds with the bilayer than K-KR12. The average lifetimes of these peptide-bilayer hydrogen bonds (Table 2) were significantly longer with R-KR12 than K-KR12, regardless of the bilayer composition. Atomic partial charge strength was the greatest indicator of the average hydrogen bond lifetime, as mutK-KR12, dmR-KR12, mR-KR12, and R-KR12 all had similar, statistically-indistinguishable, bond lifetimes. These results indicate that the strength of the atomic partial charges greatly influenced the average number of hydrogen bonds formed, allowing arginine to form stronger, more stable hydrogen bonds that persisted longer than their lysine counterparts.

3.3. MM/GBSA results support observed binding trends

MM/GBSA calculations are prone to overestimating binding affinities [64]; therefore we interpret the values in a qualitative, rather than quantitative, manner. Estimates of the peptide/bilayer binding energies follow the same general trend as the hydrogen bond analysis and peptide-bilayer association distance (Table 2). In particular, the MM/GBSA analysis substantiates the observation that K-KR12 does not bind stably with the pure POPC bilayer, with an estimated binding energy of 1.2 ± 1.5 kcal/mol. R-KR12 had only a moderately favorable binding with the pure POPC bilayer, in accordance with the greater percent association and number of hydrogen bonds seen in those simulations. Additionally, in simulations with the POPC/POPG bilayer the same trend was observed as in the hydrogen bond analysis, with K-KR12 exhibiting the least favorable binding energy and R-KR12 having the greatest binding propensity. The charge-mutant K-KR12 and methylated R-KR12s displayed intermediate values that, despite the significantly different hydrogen bonding capabilities of these peptides, are statistically indistinguishable from each other. These results suggest that, while the decreased hydrogen bonding capabilities caused by methylation only slightly affected the ability of these peptides to associate with the bilayer, they had a much more measurable effect on the energetics of that association.

3.4. Peptide insertion induces local bilayer thinning

In all simulations, the lipid bilayers displayed average thicknesses and lipid areas that are in agreement with previous experiments [65–67] and simulations [68–71], and these properties for the bilayer as a whole were largely unaffected by peptide binding (see Section S1.2 and Table S4). However, when the peptide was stably inserted in the headgroup region, decreased lipid sampling (Figure S6) and localized bilayer thinning were observed near the peptide (Fig. 5). Perturbations were most pronounced in the upper leaflet where the peptide was inserted, with observed deviations of up to 1.2 Å from the average leaflet position (Figures S7–S11). Though not as prominent as perturbations to the upper leaflet, a slight bulging out was observed in the lower leaflet in regions directly below the peptide. This concomitant thinning and bulging is similar to the initial stage of bilayer deformation observed in simulations of penetratin aggregates by Yesylevskyy et al. [72]. In the absence of the peptide, variations in thickness were mostly uncoupled between leaflets (Figure S7). Additionally, slight clustering of anionic lipids

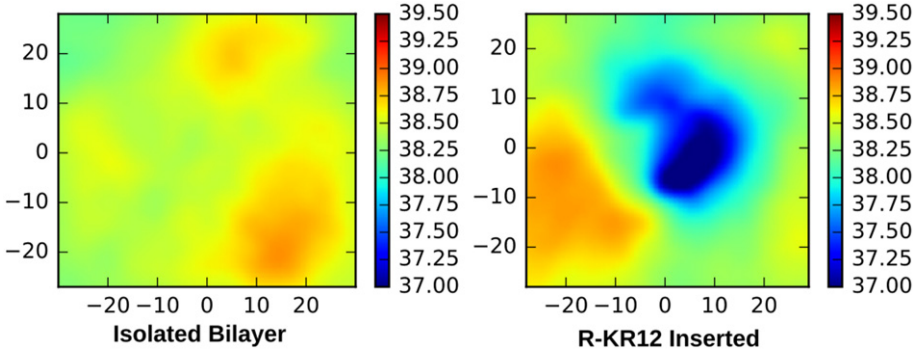

Fig. 5. Left: Thickness map for the POPC/POPG bilayer with no peptide present, averaged over a 1.0 μs simulation of the pre-equilibrated POPC/POPG bilayer. Right: Thickness map when the R-KR12 peptide is inserted into the POPC/POPG bilayer, averaged over the last 1.0 μs of the extended R-KR12/POPC/POPG simulation. Bilayer thickness is reported in Å. Peptide insertion induces bilayer thinning in the region around the peptide.

was observed when the peptide was inserted into the headgroup region (Figures S12 and S13).

3.5. Bilayer presence influences peptide structure

Potential of mean force (PMF) calculations show that the conformations of both K-KR12 and R-KR12 are similarly influenced by their bilayer interactions (Figs. 6 and S14). All PMFs had good convergence in the timescales simulated (Figures S15–S18). When free in solution, both peptides exhibited substantial conformational freedom with low barriers separating highly helical and unfolded states. Unfolded (low helicity) states for both peptides included a wide range of end-to-end distances, ranging from cyclic conformations to highly extended ones; this degeneracy further highlights the importance of using more than one collective variable to comprehensively sample the conformational space.

The energy minimum for both K-KR12 and R-KR12 corresponds to a cyclic conformation, characterized by alpha ~0.35 and a very small end-to-end distance (d < 4 Å), where the charged termini of the peptide interact directly. Cyclic structures were also present at larger distal separations of 6–10 Å, where the primary interaction was between the cationic side chain of residue 1 and the charged C-terminus of the peptide. Due to the stronger hydrogen bonding properties of arginine, this cyclic structure is more favored in the R-KR12 peptide than the K-KR12 peptide as evidenced by the lower energy values in the R-KR12 PMF. In both K-KR12 and R-KR12, a slight energy barrier exists at an end-to-end distance of 4–5 Å, which corresponds to too great of a separation distance for these direct termini interactions but too close for the side chain of residue 1 and the C-terminus to interact without significant distortion to the side chain conformation.

Insertion into the headgroup region of the bilayer caused both peptides to adopt a helical conformation, with minima occurring at an alpha value of 0.77. This strong tendency towards helicity restricted the accessible end-to-end distances, with minima around 17 Å for both systems. The helical peptide is noticeably amphipathic, with the five nonpolar residues partitioned on one face of the helix and the seven polar/charged residues on the opposite face (Fig. 7b). This conformation is preferred when inserted in the bilayer, as it promotes favorable interactions of the nonpolar residues with the lipid tails, and the charged/polar residues with the solvent and charged moieties in the lipid headgroups (Fig. 7a). This amphipathic helical structure of the inserted peptides is in close agreement with the NMR ensemble of KR-12 associated with D8PG reported by Wang [29], indicating that this conformation is not unique to the POPC/POPG bilayer mixture used here.

4. Discussion

The structural makeup of K-KR12 and R-KR12 is similar to one another in many ways. Both peptides have the same net charge of +4 coming from the five cationic residues and one aspartic acid. The free energy calculations performed here show that both peptides are primarily unstructured in solution, and preferentially fold into a three turn amphipathic α-helix when inserted in the bilayer headgroup region. The unstructured nature observed in our simulations is consistent with circular dichroism (CD) measurements that reveal a random coil conformation in solution for KR-12 [28], and for R-KR12 and K-KR12 mutants [13]. Additionally, the helical conformation that both peptides adopt in the POPC/POPG bilayer is in close agreement with the ensemble of NMR structures reported by

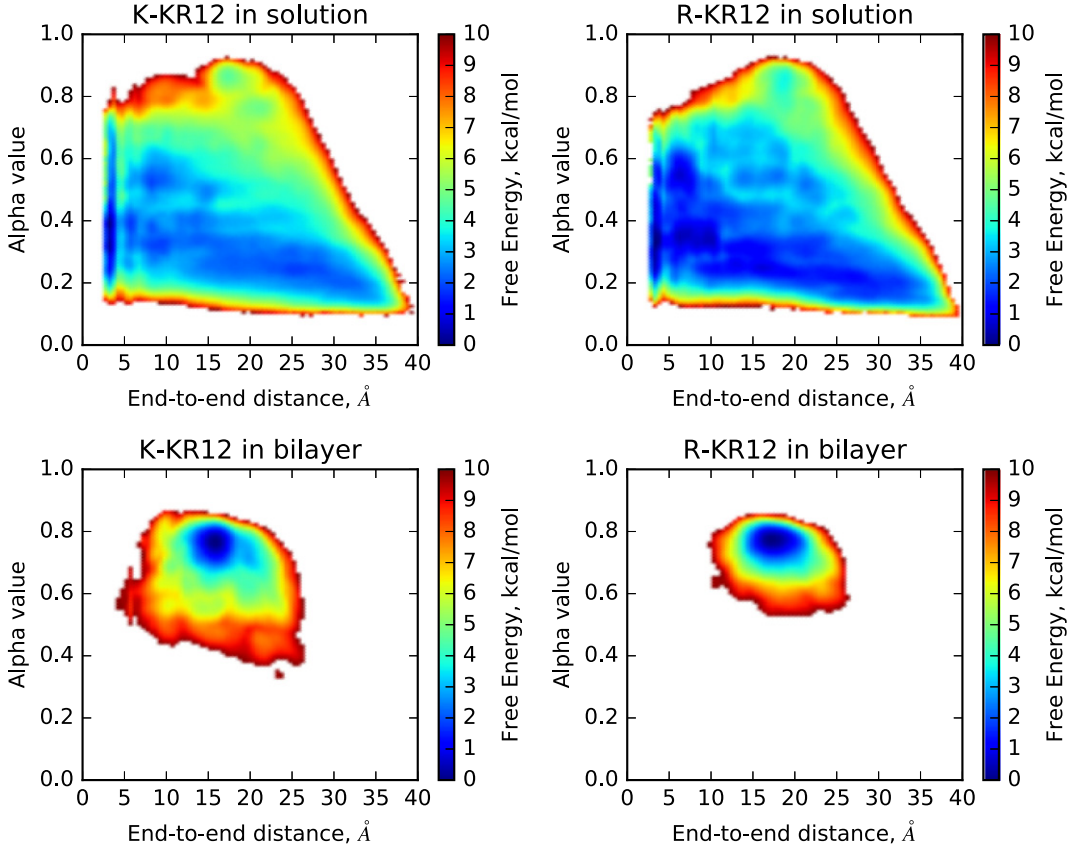

Fig. 6. Two-dimensional PMFs for K-KR12 and R-KR12, both in solution and inserted in the POPC/POPG bilayer. While both peptides are unfolded in solution, insertion into the bilayer promoted folding into an alpha helical state.

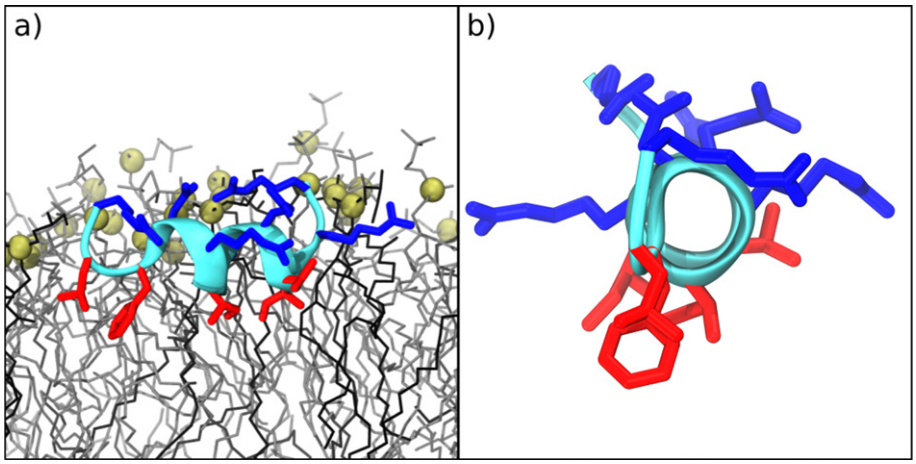

Fig. 7. Snapshots of R-KR12 inserted in the headgroup region of the POPC/POPG bilayer, highlighting the amphipathic nature of the helical peptide. a) Edge-on view of the inserted peptide with polar or charged residues in blue and nonpolar residues in red. POPC is shown in gray and POPG in black, with phosphorus atoms of both lipids depicted as gold spheres. Water and hydrogen atoms are not shown in this representation. b) View down the helix of the peptide, same frame as in (a), rotated 90° about the bilayer normal. Water, lipids, and hydrogen atoms have been removed for clarity.

Wang [29] of KR-12 associated with D8PG micelles. CD spectra from Mishra et al. of the three peptides (KR-12, K-KR12, and R-KR12) in D8PG micelles show a high percentage of α-helical content for all three, with R-KR12 being the most helical at 67%, and K-KR12 the least at 47% [13]. The PMFs presented here both have minima at the same, slightly higher, helical values of $\alpha = 0.77$. This discrepancy may be attributed to the different affinities of these peptides for anionic bilayers; R-KR12 binds more strongly and inserts more readily than K-KR12, meaning that the ensemble of K-KR12 peptides measured in the CD experiments likely contained more peptides on the surface of the micelles or free in solution than R-KR12. This difference in the fractional peptide locations could lead to a K-KR12 CD spectrum that has more random coil characteristics than the KR12 or R-KR12 spectra, which is indeed what Mishra et al. report [13]. Finally, we note that this phenomenon of membrane induced folding is not unique to LL-37 or KR-12; it has been observed in a multitude of other AMPs [1,3,4,73] and CPPs [5].

In the simulations performed here, neither K-KR12 nor R-KR12 had stable, long-term interactions with the pure POPC bilayer. Both peptides, however, interacted strongly with the POPC/POPG bilayer, highlighting the importance of anionic lipids in the initial membrane attraction. This result agrees with experiment, as KR-12 is known to be active against Gram-negative [13,28,29] and certain Gram-positive [28] bacteria, but not substantially cytotoxic or hemolytic [13,28,29]. In addition, R-KR12 has been shown to be more active against, and better able to penetrate, the inner membrane of *E. coli* than K-KR12 [13]. This is likely due to its higher propensity for hydrogen bonding with the bilayer, which resulted in the considerably longer interaction times and more favorable binding affinities we observed here.

Simulations with peptides containing methylated arginines or charge-mutated lysines were performed to help distinguish effects associated with the number of hydrogen bonds formed from those related to the cationic charge distribution. Despite their differing hydrogen bond capacities, mutK-KR12, dmR-KR12, and mR-KR12 formed a comparable number of peptide-bilayer hydrogen bonds and had the same decrease in bond number relative to R-KR12. Additionally, all three mutant peptides had the same bilayer binding energy, which was intermediate between the strong binding of R-KR12 and the weaker binding of K-KR12. Despite these differences, both methylated peptides displayed similar long-term bilayer interactions to those observed in the R-KR12 simulations, characterized by rare bilayer dissociation on the hundreds of ns timescale, large percent bilayer association compared to K-KR12, and bilayer interactions mediated by all five cationic side chains rather than just the first two residues leading to the peptide being held more closely to the bilayer surface. The strong similarity between the binding properties of the mutK-KR12 peptide and the methylated mutants highlights that, while factors such as side chain geometry and hydrophobicity may have some effect on bilayer interactions, the predominant driving force behind the disparate effects of arginine and lysine residues is the different charge distributions in the residues. Overall, these results suggest that, rather than being a simple function of the number of hydrogen bond donors, initial binding to and insertion in the membrane is affected by the cationic charge distribution, which contributes to the strength of the hydrogen bonds formed.

Though methylated arginine moieties are able to give some insight into the first stage of membrane disruption or translocation - the initial attraction to and partitioning into the bilayer - the decreased hydrogen bonding capabilities and increased hydrophobic bulk of these residues may hinder these processes. Indeed, experimental evidence suggests that guanidinium hydrogen bonding plays an important role in membrane translocation or disruption. Experimental studies of octa-arginine cellular uptake demonstrated that monomethylation reduced uptake by 80% and asymmetric dimethylation reduced uptake by greater than 95% when compared to the unmethylated octamer [74]. Additionally, symmetric dimethylation of all four arginine residues in the AMP tritrpticin decreased its capacity for both permeabilizing and disrupting PC:PG membranes, though its antimicrobial activity and ability to insert into the membrane remained intact [6], which is consistent with our observation that bilayer insertion is dependent more on the cationic charge distribution.

The importance of strong partial charges in the insertion process could help explain why arginine-rich AMPs tend to be more toxic to both prokaryotic and eukaryotic cells than their lysine-rich counterparts. Methylation of arginine residues in AMPs provides a unique way to study the effects of hydrogen bond capacity without significantly disrupting the charge distribution of the moiety. We expect that future experimental work with methylated KR-12 mutants will show a decreased cytotoxicity and hemotoxicity compared to R-KR12 while still retaining most or all of the antimicrobial properties. The work presented here focused on the initial partitioning of the peptide into the bilayer; further work must be done in order to better understand the role of hydrogen bonding and charge distribution in membrane translocation of KR-12 and LL-37. Overall, these results

help elucidate the greater toxicity of arginine-rich AMPs and offer insights for designing more potent synthetic AMPs in the future.

Transparency document

The Transparency document associated with this article can be found, in online version.

Acknowledgments

The authors thank Dr. David Gidalevitz for his valuable discussions concerning the work presented here. Research reported in this publication was supported by the National Institute of General Medical Sciences of the National Institutes of Health [grant no. R35GM119647], as well as a Pritzker Foundation Fellowship to A. R.. The content is solely the responsibility of the authors and does not necessarily represent the official views of the National Institutes of Health. This work used the Extreme Science and Engineering Discovery Environment (XSEDE) [75], which is supported by the National Science Foundation grant number ACI-1053575.

Appendix A. Supplementary data

Supplementary data to this article can be found online at http://dx.doi.org/10.1016/j.bbamem.2017.06.002.

References

[1] M. Zasloff, Antimicrobial peptides of multicellular organisms, Nature 415 (6870) (2002) 389–395.
[2] D.M. Bowdish, D.J. Davidson, Y.E. Lau, K. Lee, M.G. Scott, R.E. Hancock, Impact of LL-37 on anti-infective immunity, J. Leukoc. Biol. 77 (4) (2005) 451–459.
[3] R.E. Hancock, H.G. Sahl, Antimicrobial and host-defense peptides as new anti-infective therapeutic strategies, Nat, Biotechnol. 24 (12) (2006) 1551–1557.
[4] Y. Shai, Mechanism of the binding, insertion and destabilization of phospholipid bilayer membranes by alpha-helical antimicrobial and cell non-selective membrane-lytic peptides, Biochim, Biophys. Acta 1462 (1-2) (1999) 55–70.
[5] P. Wadhwani, R.F. Epand, N. Heidenreich, J. Burck, A.S. Ulrich, R.M. Epand, Membrane-active peptides and the clustering of anionic lipids, Biophys. J. 103 (2) (2012) 265–274.
[6] L.T. Nguyen, L. de Boer, S.A. Zaat, J. Vogel, Investigating the cationic side chains of the antimicrobial peptide tritrpticin: hydrogen bonding properties govern its membrane-disruptive activities, Biochim. Biophys. Acta 1808 (9) (2011) 2297–2303.
[7] R.A. Llenado, C.S. Weeks, M.J. Cocco, J. Ouellette, Electropositive charge in alpha-defensin bactericidal activity: functional effects of Lys-for-Arg substitutions vary with the peptide primary structure, Infect. Immun. 77 (11) (2009) 5035–5043.
[8] S.A. Muhle, J.P. Tam, Design of Gram-negative selective antimicrobial peptides, Biochemistry 40 (19) (2001) 5777–5785.
[9] Y. Tokunaga, T. Niidome, T. Hatakeyama, H. Aoyagi, Antibacterial activity of bactenecin 5 fragments and their interaction with phospholipid membranes, J. Pept. Sci. 7 (6) (2001) 297–304.
[10] I. Nakase, S. Okumura, S. Katayama, H. Hirose, S. Pujals, H. Yamaguchi, S. Arakawa, S. Shimizu, S. Futaki, Transformation of an antimicrobial peptide into a plasma membrane-permeable, mitochondria-targeted peptide via the substitution of lysine with arginine, Chem. Commun. (Camb.) 48 (90) (2012) 11097–11099.
[11] S.T. Yang, S.Y. Shin, C.W. Lee, Y.C. Kim, K.S. Hahm, J.I. Kim, Selective cytotoxicity following Arg-to-Lys substitution in tritrpticin adopting a unique amphipathic turn structure, FEBS Lett. 540 (1-3) (2003) 229–233.
[12] A. Bonucci, E. Balducci, M. Martinelli, R. pogni, Human neutrophil peptide 1 variants bearing arginine modified cationic side chains: effects on membrane partitioning, Biophys Chem. 190-191 (2014) 32–40.
[13] B. Mishra, R.F. Epand, R.M. Epand, G. Wang, Structural location determines functional roles of the basic amino acids of KR-12, the smallest antimicrobial peptide from human cathelicidin LL-37, RSC Adv 3 (42) (2013) 19560–19571.
[14] K. Andreev, C. Bianchi, J.S. Laursen, L. Citterio, L. Hein-Kristensen, L. Gram, I. Kuzmenko, C.A. Olsen, D. Gidalevitz, Guanidino groups greatly enhance the action of antimicrobial peptidomimetics against bacterial cytoplasmic membranes, Biochim. Biophys. Acta 1838 (10) (2014) 2492–2502.
[15] D.J. Mitchell, D.T. Kim, L. Steinman, C.G. Fathman, J.B. Rothbard, Polyarginine enters cells more efficiently than other polycationic homopolymers, J. Pept. Res. 56 (5) (2000) 318–325.
[16] A.D. Robison, S. Sun, M.F. Poyton, G.A. Johnson, J.P. Pellois, P. Jungwirth, M. Vazdar, P.S. Cremer, Polyarginine interacts more strongly and cooperatively than polylysine with phospholipid bilayers, J. Phys. Chem. B 120 (35) (2016) 9287–9296.
[17] J. Turner, Y. Cho, N.N. Dinh, A.J. Waring, R.I. Lehrer, Activities of LL-37, a cathelin-associated antimicrobial peptide of human neutrophils, Antimicrob. Agents Chemother. 42 (9) (1998) 2206–2214.
[18] U.H. Durr, U.S. Sudheendra, A. Ramamoorthy, LL-37, The only human member of the cathelicidin family of antimicrobial peptides, Biochim. Biophys. Acta 1758 (9) (2006) 1408–1425.
[19] Z. Oren, J.C. Lerman, G.H. Gudmundsson, B. Agerberth, Y. Shai, Structure and organization of the human antimicrobial peptide LL-37 in phospholipid membranes: relevance to the molecular basis for its non-cell-selective activity, Biochem. J. 341 (Pt 3) (1999) 501–513.
[20] K.A. Henzler Wildman, D.K. Lee, A. Ramamoorthy, Mechanism of lipid bilayer disruption by the human antimicrobial peptide, LL-37, Biochemistry 42 (21) (2003) 6545–6558.
[21] K.A. Henzler-Wildman, G.V. Martinez, M.F. Brown, A. Ramamoorthy, Perturbation of the hydrophobic core of lipid bilayers by the human antimicrobial peptide LL-37, Biochemistry 43 (26) (2004) 8459–8469.
[22] F. Neville, M. Cahuzac, O. Konovalov, Y. Ishitsuka, K.Y. Lee, I. Kuzmenko, G.M. Kale, D. Gidalevitz, Lipid headgroup discrimination by antimicrobial peptide LL-37: insight into mechanism of action, Biophys. J. 90 (4) (2006) 1275–1287.
[23] B. Agerberth, J. Charo, J. Werr, B. Olsson, F. Idali, L. Lindbom, R. Kiessling, H. Jornvall, H. Wigzell, G.H. Gudmundsson, The human antimicrobial and chemotactic peptides LL-37 and alpha-defensins are expressed by specific lymphocyte and monocyte populations, Blood 96 (9) (2000) 3086–3093.
[24] J.W. Larrick, M. Hirata, R.F. Balint, J. Lee, J. Zhong, S.C. Wright, Human CAP18: a novel antimicrobial lipopolysaccharide-binding protein, Infect. Immun. 63 (4) (1995) 1291–1297.
[25] C.D. Ciornei, T. Sigurdardottir, A. Schmidtchen, M. Bodelsson, Antimicrobial and chemoattractant activity, lipopolysaccharide neutralization, cytotoxicity, and inhibition by serum of analogs of human cathelicidin LL-37, Antimicrob. Agents Chemother. 49 (7) (2005) 2845–2850.
[26] Z. Zhang, G. Cherryholmes, J.E. Shively, Neutrophil secondary necrosis is induced by LL-37 derived from cathelicidin, J. Leukoc. Biol. 84 (3) (2008) 780–788.
[27] J. Sall, M. Carlsson, O. Gidlof, A. Holm, J. Humlen, J. Ohman, D. Svensson, B.O. Nilsson, D. Jonsson, The antimicrobial peptide LL-37 alters human osteoblast Ca2+ handling and induces Ca2+-independent apoptosis, J. Innate Immun. 5 (3) (2013) 290–300.
[28] B. Jacob, I.S. Park, J.K. Bang, S.Y. Shin, Short KR-12 analogs designed from human cathelicidin LL-37 possessing both antimicrobial and antiendotoxic activities without mamMalian cell toxicity, J. Pept. Sci. 19 (11) (2013) 700–707.
[29] G. Wang, Structures of human host defense cathelicidin LL-37 and its smallest antimicrobial peptide KR-12 in lipid micelles, J. Biol. Chem. 283 (47) (2008) 32637–32643.
[30] M. Evich, E. Stroeva, Y.G. Zheng, M.W. Germann, Effect of methylation on the side-chain pKa value of arginine, Protein Sci. 25 (2) (2016) 479–486.
[31] S. Jo, T. Kim, W. Im, Automated builder and database of protein/membrane complexes for molecular dynamics simulations, PLoS ONE 2 (9) (2007) e880.
[32] E.L. Wu, X. Cheng, S. Jo, H. Rui, K.C. Song, E.M. Davila-Contreras, Y. Qi, J. Lee, V. Monje-Galvan, R.M. Venable, J.B. Klauda, W. Im, CHARMM-GUI Membrane builder toward realistic biological membrane simulations, J. Comb. Chem. 35 (27) (2014) 1997–2004.
[33] J.B. Klauda, R.M. Venable, J.A. Freites, J.W. O'Connor, D.J. Tobias, C. Mondragon-Ramirez, I. Vorobyov, A.D. MacKerell, R.W. Pastor, Update of the CHARMM all-atom additive force field for lipids: validation on six lipid types, J. Phys. Chem. B 114 (23) (2010) 7830–7843.
[34] R.W. Pastor, A.D. Mackerell, Development of the CHARMM force field for lipids, J. Phys. Chem. Lett. 2 (13) (2011) 1526–1532.
[35] W. Humphrey, A. Dalke, K. Schulten, VMD - Visual molecular dynamics, J. Mol. Graph. 14 (1996) 33–38.
[36] W. Jorgensen, J. Chandrasekhar, J. Madura, R. Impey, M. Klein, Comparison of simple potential functions for simulating liquid water, J. Chem. Phys. 79 (2) (1983) 926–935.
[37] M. Crowley, M. Williamson, R. Walker, CHAMBER: Comprehensive support for CHARMM force fields within the AMBER software, Int. J. Quantum Chem. 109 (15) (2009) 3767–3772.
[38] A.D. MacKerell, D. Bashford, M. Bellott, R.L. Dunbrack, J.D. Evanseck, M.J. Field, S. Fischer, J. Gao, H. Guo, S. Ha, D. Joseph-McCarthy, L. Kuchnir, K. Kuczera, F.T. Lau, C. Mattos, S. Michnick, T. Ngo, D.T. Nguyen, B. Prodhom, W.E. Reiher, B. Roux, M. Schlenkrich, J.C. Smith, R. Stote, J. Straub, M. Watanabe, J. Wiorkiewicz-Kuczera, D. Yin, M. Karplus, All-atom empirical potential for molecular modeling and dynamics studies of proteins, J. Phys. Chem. B 102 (18) (1998) 3586–3616.
[39] R.B. Best, X. Zhu, J. Shim, P.E. Lopes, J. Mittal, M. Feig, A.D. Mackerell, Optimization of the additive CHARMM all-atom protein force field targeting improved sampling of the backbone phi, psi and side-chain chi1 and chi2 dihedral angles, J. Chem. Theory Comput. 8 (9) (2012) 3257–3273.
[40] R.M. Venable, Y. Luo, K. Gawrisch, B. Roux, R.W. Pastor, Simulations of anionic lipid membranes: development of interaction-specific ion parameters and validation using NMR data, J. Phys. Chem. B 117 (35) (2013) 10183–10192.
[41] K. Vanommeslaeghe, E. Hatcher, C. Acharya, S. Kundu, S. Zhong, J. Shim, E. Darian, O. Guvench, P. Lopes, I. Vorobyov, A.D. Mackerell, CHARMM general force field: a force field for drug-like molecules compatible with the CHARMM

all-atom additive biological force fields, J. Comb. Chem. 31 (4) (2010) 671–690.
[42] C.G. Mayne, J. Saam, K. Schulten, E. Tajkhorshid, J.C. Gumbart, Rapid parameterization of small molecules using the Force Field Toolkit, J. Comb. Chem. 34 (32) (2013) 2757–2770.
[43] O. Guvench, A.D. MacKerell, Automated conformational energy fitting for force-field development, J. Mol. Model. 14 (8) (2008) 667–679.
[44] M.J. Frisch, Gaussian09 Revision D.01, Gaussian Inc Wallingford CT, 2009.
[45] H.J.C. Berendsen, J.P.M. Postma, W.F. van Gunsteren, A. DiNola, J.R. Haak, Molecular dynamics with coupling to an external bath, J. Chem. Phys. 81 (8) (1984) 3684–3690.
[46] V. Krautler, W.F. Van Gunsteren, P.H. Hunenberger, A. fast, SHAKE: algorithm to solve distance constraint equations for small molecules in molecular dynamics simulations, J. Comb. Chem. 22 (2001) 501–508.
[47] J. Lee, X. Cheng, J.M. Swails, M.S. Yeom, P.K. Eastman, J.A. Lemkul, S. Wei, J. Buckner, J.C. Jeong, Y. Qi, S. Jo, V.S. Pande, D.A. Case, C.L. Brooks, A.D. MacKerell, J.B. Klauda, W. Im, CHARMM-GUI input generator for NAMd, GROMACS, AMBER, OpenMM, and CHARMM/OpenMM simulations using the CHARMM36 additive force field, J. Chem. Theory Comput. 12 (1) (2016) 405–413.
[48] T. Darden, D. York, L. Pedersen, Particle mesh Ewald - an N.log(N) method for Ewald sums in large systems, J. Chem. Phys. 98 (1993) 10089–10092.
[49] D.A. Case, T.E. Cheatham, T. Darden, H. Gohlke, R. Luo, K.M. Merz, A. Onufriev, C. Simmerling, B. Wang, R.J. Woods, The Amber biomolecular simulation programs, J. Comb. Chem. 26 (16) (2005) 1668–1688.
[50] G.M. Torrie, J.P. Valleau.
[51] J.C. Phillips, R. Braun, W. Wang, J. Gumbart, E. Tajkhorshid, E. Villa, C. Chipot, R.D. Skeel, L. Kale, K. Schulten, Scalable molecular dynamics with NAMD, J. Comb. Chem. 26 (16) (2005) 1781–1802.
[52] G. Fiorin, M.L. Klein, J. Hénin, Using collective variables to drive molecular dynamics simulations, Mol. Phys. 111 (22-23) (2013) 3345–3362.
[53] A. Hazel, C. Chipot, J.C. Gumbart, Thermodynamics of deca-alanine folding in water, J. Chem. Theory Comput. 10 (7) (2014) 2836–2844.
[54] Y. Sugita, A. Kitao, Y. Okamoto, Multidimensional replica-exchange method for free-energy calculations, J. Chem. Phys. 113 (15) (2000) 6042–6051.
[55] S. Feller, Y. Zhang, R. Pastor, B. Brooks, Constant pressure molecular dynamics simulation: the Langevin pison method, J. Chem. Phys. 103 (11) (1995) 4613–4621.
[56] S. Kumar, D. Bouzida, R. Swendsen, P. Kollman, J. Rosenberg, The weighted histogram analysis method for free-energy calculations on Biomolecules, J. Comb. Chem. 13 (8) (1992) 1011–1021.
[57] A. Grossfield, WHAM: The Weighted Histogram Analysis Method, Version 2.0.9, 2013, http://membrane.urmc.rochester.edu/content/wham.
[58] I.V. Khavrutskii, J. Dzubiella, J.A. McCammon, Computing accurate potentials of mean force in electrolyte solutions with the generalized gradient-augmented harmonic fourier beads method, J. Chem. Phys. 128 (4) (2008) 044106.
[59] R. Guixa-Gonzalez, I. Rodriguez-Espigares, J.M. Ramirez-Anguita, P. Carrio–Gaspar, H. Martinez-Seara, T. Giorgino, J. Selent, M, EMBPLUGIN: studying membrane complexity in VMD, Bioinformatics 30 (10) (2014) 1478–1480.
[60] T.D. Romo, A. Grossfield, LOOS: an extensible platform for the structural analysis of simulations, Conf. Proc. IEEE Eng. Med. Biol. Soc. 2009 (2009) 2332–2335.
[61] B.R. Miller, T.D. McGee, J.M. Swails, N. Homeyer, H. Gohlke, A.E. Roitberg, MMPBSA.Py: an efficient program for end-state free energy calculations, J. Chem. Theory Comput. 8 (9) (2012) 3314–3321.
[62] A. Onufriev, D. Bashford, D.A. Case, Exploring protein native states and large-scale conformational changes with a modified generalized born model, Proteins 55 (2) (2004) 383–394.
[63] W.F. Bennett, C.K. Hong, Y. Wang, D.P. Tieleman, Antimicrobial peptide simulations and the influence of force field on the free energy for pore formation in lipid bilayers, J. Chem. Theory Comput. 12 (9) (2016) 4524–4533.
[64] S. Genheden, U. Ryde, The MM/PBSA and MM/GBSA methods to estimate ligand-binding affinities, Expert Opin. Drug Discovery 10 (5) (2015) 449–461.
[65] P.A. Hyslop, B. Morel, R.D. Sauerheber, Organization and interaction of cholesterol and phosphatidylcholine in model bilayer membranes, Biochemistry 29 (4) (1990) 1025–1038.
[66] N. Kucerka, S. Tristram-Nagle, J.F. Nagle, Structure of fully hydrated fluid phase lipid bilayers with monounsaturated chains, J. Membr. Biol. 208 (3) (2005) 193–202.
[67] J. Pan, D. Marquardt, F.A. Heberle, N. Ku?erka, J. Katsaras, Revisiting the bilayer structures of fluid phase phosphatidylglycerol lipids: accounting for exchangeable hydrogens, Biochim. Biophys. Acta 1838 (11) (2014) 2966–2969.
[68] S.A. Pandit, S.W. Chiu, E. Jakobsson, A. Grama, H.L. Scott, Cholesterol surrogates: a comparison of cholesterol and 16:0 ceramide in POPC bilayers, Biophys. J. 92 (3) (2007) 920–927.
[69] P. Jurkiewicz, L. Cwiklik, L. Cwiklik, A. Vojti?kova, P. Jungwirth, M. Hof, Structure, dynamics, and hydration of POPC/POPS bilayers suspended in NaCl, KCl, and CsCl solutions, Biochim. Biophys. Acta 1818 (3) (2012) 609–616.
[70] A.A. Gurtovenko, I. Vattulainen, Effect of NaCl and KCl on phosphatidylcholine and phosphatidylethanolamine lipid membranes: insight from atomic-scale simulations for understanding salt-induced effects in the plasma membrane, J. Phys. Chem. B 112 (7) (2008) 1953–1962.
[71] L. Janosi, A.A. Gorfe, Simulating POPC and POPC/POPG bilayers: conserved packing and altered surface reactivity, J. Chem. Theory Comput. 6 (10) (2010) 3267–3273.
[72] S. Yesylevskyy, S.J. Marrink, A.E. Mark, Alternative mechanisms for the interaction of the cell-penetrating peptides penetratin and the TAT peptide with lipid bilayers, Biophys. J. 97 (1) (2009) 40–49.
[73] Y. Wang, D.E. Schlamadinger, J.E. Kim, J.A. McCammon, Comparative molecular dynamics simulations of the antimicrobial peptide CM15 in model lipid bilayers, Biochim. Biophys. Acta 1818 (5) (2012) 1402–1409.
[74] J.B. Rothbard, T.C. Jessop, R.S. Lewis, B.A. Murray, P.A. Wender, Role of membrane potential and hydrogen bonding in the mechanism of translocation of guanidinium-rich peptides into cells, J. Am. Chem. Soc. 126 (31) (2004) 9506–9507.
[75] J. Towns, T. Cockerill, M. Dahan, I. Foster, K. Gaither, A. Grimshaw, V. Hazlewood, S. Lathrop, D. Lifka, G.D. Peterson, R. Roskies, J.R. Scott, N. Wilkins-Diehr, Xsede: accelerating scientific discovery, Comput. Sci. Eng. 16 (5) (2014) 62–74. http://dx.doi.org/10.1109/MCSE.2014.80.